

# Bayesian Single-Epoch Photometric Classification of Supernovae

Dovi Poznanski and Dan Maoz

*School of Physics & Astronomy, Tel-Aviv University, Tel-Aviv 69978, Israel*

dovip,dani @wise.tau.ac.il

and

Avishay Gal-Yam<sup>1</sup>

*Astronomy Department, MS 105-24, California Institute of Technology, Pasadena, CA 91125*

avishay@astro.caltech.edu

## ABSTRACT

Ongoing supernova (SN) surveys find hundreds of candidates, that require confirmation for their use as standard candles, to measure the cosmic supernova and star formation rates, to constrain progenitor models, and to track the contribution of supernovae (SNe) to metal enrichment. Traditional classification based on followup spectroscopy of all candidates is virtually impossible for these large samples. We present an automatic Bayesian classifying algorithm for supernovae, the SN-ABC. We rely solely on single-epoch multiband photometry and host-galaxy (photometric) redshift information to sort SN candidates into the two major types, Ia and core-collapse supernovae. We test the SN-ABC performance on published samples of SNe from the SNLS and GOODS projects that have both broad-band photometry and spectroscopic classification (so the true type is known). The SN-ABC correctly classifies up to 97% (85%) of the type Ia (II-P) SNe in SNLS, and similar fractions of the GOODS SNe, depending on photometric redshift quality. We further test our method on large artificial samples to explore possible biases, and find that, in deep surveys, SNe Ia are best classified at redshifts  $z \gtrsim 0.6$ , or when near maximum, with success rates of the order of 95%. Core-collapse SNe are best recognized several weeks after maximum, or at  $z \lesssim 0.6$ , and reach success rates near 80%. The SN-ABC also allows

---

<sup>1</sup>Hubble Fellow.

the rejection of SN “impostors” such as active galactic nuclei (AGNs), with half of of the AGNs we simulate rejected by the algorithm. We tested the SN-ABC on single-epoch photometric data with observations in one to four bands, and find that while SNe may be classified with one or two bands, three bands are necessary for obtaining a reasonable reliability, and AGN rejection. On the other hand, observations in a fourth band may not be worth the added observational cost, for classification purposes. Our algorithm also supplies a good estimator of the quality of the classification, which is valuable for error estimation. In a separate paper, we use our method to classify a new sample of high- $z$  SNe that we have found in the Subaru Deep Field.

*Subject headings:* supernovae: general

## 1. Introduction

Supernovae (SNe) are usually subdivided into different types, based on spectroscopic or photometric criteria (e.g., Filippenko 1997). The primary physical distinction among the common supernova (SN) types separates core collapse SNe (CC-SNe), that originate from the collapse of a massive star (e.g., Woosley & Janka 2005), from type-Ia SNe (SNe Ia), for which there are competing scenarios, generally involving a thermonuclear runaway in a degenerate system (e.g., Hillebrandt & Niemeyer 2000).

Recent technological advances in wide field imaging and in automation capabilities, combined with a growing interest in transient phenomena, have led to numerous surveys that find hundreds of SNe. These surveys search for SNe nearby (Filippenko et al. 2001; Wood-Vasey et al. 2004), at intermediate redshifts (Dilday et al. 2005; Cappellaro et al. 2005), and at high redshifts (Astier et al. 2006; Riess et al. 2004a; Sollerman et al. 2005, Poznanski et al., in preparation). While most ongoing SN searches focus on the use of SNe Ia as standard candles for cosmological applications (Riess et al. 2004a; Astier et al. 2006), large SN samples can be used also to study the statistical properties of the SNe themselves, and to measure their rates as a function of cosmic time (e.g., Maoz & Gal-Yam 2004; Dahlen et al. 2004). Because the lifetimes of massive stars are short compared to cosmological timescales, the rate of CC-SNe is expected to follow the star formation history, and thus could provide an independent measure of this function (e.g., Dahlén & Fransson 1999). The rate of SNe Ia is linked to star formation through a more complicated evolutionary process that depends on the nature of the progenitor systems. Measurement of the SN Ia rate may therefore constrain possible progenitor models (e.g., Gal-Yam & Maoz 2004; Strolger et al. 2004; Scannapieco & Bildsten 2005; Mannucci et al. 2005, 2006; Sullivan et al. 2006b; Förster et al. 2006).

Future projects such as Pan-STARRS (Kaiser et al. 2005), LSST (Stubbs et al. 2004), and SNAP (Aldering 2005), promise to increase the yield of SNe by orders of magnitude, especially at intermediate and high redshifts. All of the SN studies above require large, well-defined samples of SNe with determined types and redshifts. The common methodology of attempting to obtain spectroscopic followup of every SN candidate, in order to determine its type, its redshift (based on the host spectrum or from the SN spectrum itself), and possibly other characteristics, is unsuitable for this plethora of SNe, due to their faintness, sheer numbers, or both. For this reason, current surveys usually focus on subsets of the SN candidates for which spectroscopic observations can be obtained. Ongoing surveys already employ some photometric criteria for prioritizing followup, but usually not for definitive classification, as we discuss below.

In Poznanski et al. (2002) and Gal-Yam et al. (2004), we showed, using color-color diagrams, that given a known redshift, different types of SNe can often be distinguished based on colors alone. Our method and webtool<sup>1</sup> have been used, among others, by Rajala et al. (2005), to classify nearby SNe, by Gal-Yam et al. (2005) to choose objects for followup prior to spectroscopy, and by Strolger et al. (2004) for high redshift CC-SN identification. The approach has been developed further by several studies. Riess et al. (2004b) showed that, at high redshift, it might be even easier to distinguish, near maximum light, between SNe Ia and CC-SNe, by virtue of the difference in the rest frame UV emission between these two classes of objects. Johnson & Crotts (2006) investigated further the color-magnitude based classification of intermediate redshift SNe with different filter sets and both with and without redshift information. Sullivan et al. (2006a) introduced the use of automatic photometric classification as part of the reduction pipeline of the SN Legacy Survey (SNLS; Astier et al. 2006), using two to three early light-curve points. The objective was mainly to recognize SNe Ia, with a minimum of false positives and selection biases, and thus to prioritize targets for followup spectroscopy. Barris & Tonry (2006) fit complete light curves and applied various quality cuts in order to recognize SNe Ia among the various transients they found in their survey (see also Barris & Tonry 2004).

In this paper, we present an algorithm, the SN Automatic Bayesian Classifier (SN-ABC), intended for automatic classification of SNe using single-epoch photometry and whatever redshift information is available. The main novelty of our algorithm lies in the flexibility of the Bayesian approach, which allows us to analyze SNe from different surveys, with different depths and types of redshift information, to incorporate fully all the available information on each object, and to propagate correctly the unknowns. As a proof of concept, we focus

---

<sup>1</sup><http://wise-obs.tau.ac.il/~dovip/typing/>

on single-epoch photometry in three bands, but the method can be straightforwardly implemented with multiply sampled light curves with other photometric setups. As we will show, SNe can be classified reliably even with meager input data, and therefore numerous SNe can be found and analyzed at a relatively low cost in telescope time.

We test our method on light curves, recently released by the SNLS, of 71 SNe Ia and five “plateau” type (II-P) SNe (Astier et al. 2006; Nugent et al. 2006), and on the sample of 42 SNe found during the GOODS campaign (Dahlen et al. 2004). A third sample of simulated SN data is used to investigate potential biases and the efficiency of the method as a function of SN and sample parameters. In a separate paper (Poznanski et al., in preparation), we use our method to classify a sample of SNe we have found in the Subaru Deep Field (SDF; Kashikawa et al. 2004), and to measure the rates of Ia and CC SNe at high redshift based on this dataset.

Shortly prior to submission of this paper, Kuznetsova & Connolly (2006) presented a Bayesian classification algorithm, and its application to SNLS and GOODS data. Although there are some similarities between their approach and ours, there are also some major differences. First, while they use complete light curve data, and discuss their importance, we focus on single epoch data, where information is scarce, and classification is less obvious. Second, they treat, though it is not implicit in their work, the redshift of the SN as a known quantity without any ambiguity. While this is true for most of the SNe in the training samples they (and we) use, this is certainly not the case for existing and future SN samples, where methods of photometric classification apply. In our work, while we focus on the case where photometric redshifts for the host galaxies of the SNe are available, we treat the general case, in which each object can have any possible redshift estimation, either precise (spectroscopic) or totally unavailable. In each case the uncertainties in the redshift measurement are taken into account. Finally, Kuznetsova & Connolly (2006) estimate the probabilities after marginalizing over three limited extinction scenarios, (no extinction,  $R_V = 3.1$  with  $A_V = 0.4$ , and  $R_V = 2.1$  with  $A_V = 0.4$ ). As explained in §2.2, we assume a whole range of extinction models with  $R_V = 3.1$ , and  $A_V$  between zero and one.

## 2. Method

Our general approach for SN classification relies on a Bayesian template fitting technique. Given a “prior” on the redshift of a SN candidate, we fit a set of template spectral energy distributions (SEDs) to the observed photometry of the SN. We then maximize the likelihood in order to find the characteristics of the SN, derive the evidence for the object being either a SN Ia or a CC-SN, and find its posterior redshift distribution function. We

describe below each step in detail.

## 2.1. SN Photometry and Prior (Redshift) Information

We will assume the availability of single-epoch multi-band photometry of the candidate SNe. As we will show, this is probably the minimum amount of data that can produce scientifically meaningful results, and is also the kind of information we have for the SDF (Poznanski et al., in preparation). However, this method can be easily applied to cases where more information is available, including complete multi-band light curves, with a guaranteed improvement in the results.

We further assume the existence of a prior redshift probability distribution function (z-pdf) for the SNe. Such a prior distribution would come naturally from the photometric redshifts of the host galaxies, but in principle could be from any source. Photometric redshifts are now being produced by every major extragalactic survey, and for well studied fields there may even be an available spectrum of the host galaxy, or one can be obtained later when the SN has faded. (In the Bayesian formulation, a spectroscopic redshift corresponds to a sharply peaked prior z-pdf.) In cases where there is no redshift information (e.g., because the host is too faint) one can assume a flat, or other physically motivated z-pdf.

The Bayesian approach permits a careful treatment of the unknowns, that can be propagated fully from one step of the analysis to the next. Even when the redshift is derived from spectroscopy, it can have uncertainties which are hard to propagate further in any frequentist approach. Here, we can treat self-consistently redshift information of any given quality, whether a narrow peaked z-pdf from a spectral redshift, a broad, or oddly shaped redshift distribution, including redshift limits, or even non-existent photometric redshift, all jointly analyzed. Furthermore, when interested in the redshift distribution of the SNe, one can use the full posterior redshift distribution for each object, rather than a single value derived from its peak, and thus propagate further the complete information. Finally, in “rolling searches”, where, e.g., all SNe are found when rising or near peak, one can similarly include a prior on the age of the SN, and thus improve the classification.

## 2.2. Model

We use SN templates from the updated version of the SN SED database of Nugent et al. (2002)<sup>2</sup>. These include sets of redshift  $z = 0$  spectra of SNe of different types and at different epochs, covering the NIR to the restframe UV. After experimenting with various simulations and applications to real data, most of which are presented in Sections 3 and 4, we find that the best classification, and the fewest subsequent biases, in type and redshift distributions, are achieved when only the templates for types II-P and Ia are used in the fits. As we will show in §4, we find that, with the exception of type IIn SNe (see discussion in §4), most non-II-P CC-SNe, are more similar, on average, to type II-P than to type Ia SNe. Since our main objective will be an empirical division between the two main physical classes of SNe, Ia and CC, we retain only these two types, using the II-P templates as proxies for the whole CC SN class. In general template fitting algorithms the use of many templates, including relatively rare objects, tends to damage the fit of the more common objects (e.g., Benítez 2000). In our case, adding templates for other CC-SNe, while somehow improving the classification of these types of SNe, causes many SNe Ia to be wrongly classified, and thus lowers the overall success rate of our algorithm.

Our adopted templates span a range in SN age,  $t$ , from about two weeks prior to maximum  $B$ -band light to two (three) months past maximum for the Ia (CC) SNe. Using synthetic photometry, we have scaled the template spectra to reach at maximum light the  $B$ -band absolute magnitudes in Table 1 of Dahlen et al. (2004), which are based on the works of Richardson et al. (2002), Li et al. (2001), and Tonry et al. (2003). We consider two types of intrinsic dispersion in SN properties – one in the absolute magnitude, which we take from Dahlen et al. (2004), and one in color, of 0.1 mag. The latter is consistent with what has been measured for SNe Ia by Nobili et al. (2003), Jha et al. (2006), and Ellis et al. (in preparation), while for CC-SNe we are not aware of the existence of similar published data (though see Elmhamdi et al. 2003).

We apply to the template spectra a grid of redshifts (from 0 to 2) and extinctions ( $A_V = 0 - 1$  mag) at the SN redshift, using the Cardelli, Clayton, & Mathis (1989) extinction law, with  $R_V = 3.1$ . Luminosity distances are calculated using the currently favored cosmology ( $h = 0.7, \Omega_\Lambda = 0.7, \Omega_m = 0.3$ ). Finally, we apply a range of observer-frame Galactic extinctions to the spectra, again using the reddening law of Cardelli et al. (1989).

We calculate synthetic magnitudes from the SEDs, based on the bandpasses used in the particular survey being analyzed. These bandpasses are the products of the filter transmis-

---

<sup>2</sup>available at [http://supernova.lbl.gov/~nugent/nugent\\_templates.html](http://supernova.lbl.gov/~nugent/nugent_templates.html)

sion curves, detector quantum efficiency curves, and (for ground-based data) atmospheric transmission. We thus obtain a  $5d$  data cube of model magnitudes for each type of SN as a function of redshift, age, band, host extinction, and Galactic extinction, from which we select for each object a  $4d$  cube according to the expected Galactic extinction from the maps of Schlegel, Finkbeiner, & Davis (1998). We perform all of our analysis using Vega-based magnitudes.

### 2.3. Fitting

For every SN we classify, we calculate two  $3d$  posterior likelihood matrices, one assuming it is a SN Ia, and one assuming it is a CC-SN:

$$L_{type}(z, A_V, t) = P(z) \cdot \exp \left[ - \sum_i \left( \frac{m_{\text{mod},i}(z, A_V, t) - m_i}{dm_i} \right)^2 \right],$$

with the summation being over the available bands, and denoted here by the index  $i$ .  $P(z)$  is the redshift prior,  $m_{\text{mod},i}$  are the model magnitudes computed from the templates (see §2.2),  $m_i$  are the measured magnitudes, and  $dm_i$  are the photometric errors and model dispersions summed in quadrature. In order to account for the different dispersions in the absolute magnitudes of the model SNe and their colors, we technically do not fit  $n$  magnitudes in  $n$  bands, but rather one magnitude and  $(n - 1)$  colors. We marginalize the likelihood function over the three parameters,  $z$ ,  $A_V$ , and  $t$ , and obtain the summed likelihood for each type of SN, commonly referred to in Bayesian literature (e.g., Gelman et al. 1995) as the *evidence*,

$$E_{type} = \int L_{type}(z, A_V, t) dz dA_V dt.$$

In order to classify the SNe, we define a relative evidence to express the probability that an object is a SN Ia, as

$$P_{Ia} = \frac{E_{Ia}}{E_{Ia} + E_{CC}}.$$

We also derive for each SN its posterior redshift, assuming it belongs to a given type of SN, by marginalizing the relevant likelihood function over the nuisance parameters, namely the age and the extinction. The final output is then the probability for the SN to be of type Ia, rather than being a core-collapse event, and its posterior  $z$ -pdf. In the following sections, we consider the adopted type of a SN to be the type which has a probability higher than 0.5. Naturally, the higher this probability, the more secure is the classification. We also examine the  $\chi^2$  value for the best fitting template, in order to ascertain the goodness of fit in an absolute sense, and in order to reject SN impostors, mainly active galactic nuclei (AGNs).

### 3. Tests on Real Data

We now apply our algorithm to two real data sets, SNLS and GOODS, that have photometric data of the type we are considering (e.g., SNe observed in at least three bands), and followup spectroscopy based upon which we can evaluate the performance of our method.

#### 3.1. SNLS

##### 3.1.1. *Ia SNe*

We begin with 71 published lightcurves of SNe Ia from the SNLS project<sup>3</sup>, described in Astier et al. (2006). The SNLS is a 5-year ‘rolling’ SN-Ia survey, using the MegaCam wide field imager on the 3.6 m Canada-France-Hawaii Telescope. The fields are imaged in four bands, similar to the Sloan Digital Sky Survey  $g, r, i, z$  (Fukugita et al. 1996; Astier et al. 2006), with limiting magnitudes in  $i$  of the order of 24.5 mag. The SN candidates are confirmed using spectroscopy from 8-10 m class telescopes. The SNe in our sample are all spectroscopically confirmed SNe Ia at  $z = 0.25 - 1$ , with a median of  $z = 0.6$ . Typical photometric errors are smaller than 0.1 mag. Since our main focus is on classification by means of three bands, we ignore at first  $g$ -band data (but see §4.4), and use for each SN only those data combinations which have same-day ( $\pm 1$ ) photometry in  $r, i, z$ . This produces a sample of 172 ‘objects’, extracted from 58 SNe. This selection does not affect the redshift distribution, which remains similar to the distribution of the original sample.

Since these SNe have spectroscopic redshifts, we create simulated photometric redshifts,  $z_{\text{rand}}$ , by adding to each object’s redshift a normally distributed (with zero mean and  $\sigma_1$  standard deviation) error,

$$z_{\text{rand}} = z_{\text{spec}} + \text{noise}(\sigma_1),$$

and create a Gaussian  $z$ -pdf of width  $\sigma_2$ , centered on the noise-added redshift,

$$P_{\text{phot}}(z) = \frac{1}{\sigma_2 \times \sqrt{2\pi}} \cdot \exp \left[ -\frac{(z - z_{\text{rand}})^2}{2\sigma_2^2} \right].$$

To evaluate the impact of the precision of redshift determination, we have run the SN-ABC for various combinations of  $\sigma_1$  and  $\sigma_2$  values. For every SN, we perform several specific  $z_{\text{rand}}$  realizations, and average the outcomes.

---

<sup>3</sup>available at <http://snls.in2p3.fr/conf/release/>



In Figure 1 we present the SN-ABC output  $P_{Ia}$  distributions (left) for various precisions of redshift determinations, and the posterior redshift compared to the spectroscopic one (right). We start with  $\sigma_1 = 0$  and  $\sigma_2 = 0.01$ , which can represent well-determined, i.e., spectroscopic, redshifts. In this case  $\sim 97\%$  of the SNe are correctly classified by the SN-ABC.

With  $\sigma_1 = \sigma_2 = 0.1$ , a reasonable precision for photometric redshifts in most surveys and redshift ranges (e.g., Grazian et al. 2006; Coe et al. 2006), This result remains unchanged, with 97% correctly classified SNe, and  $\sim 65\%$  having  $P_{Ia} > 0.9$ . The posterior redshift scatter is marginally reduced, compared to the constructed prior standard deviation of  $\sigma = 0.1$ , indicating that this precision in redshift is about the limit of what can be achieved with single epoch data in three bands.

For  $\sigma_1 = \sigma_2 = 0.3$ , i.e., very broadly distributed and imprecise redshifts, and probably the worst case scenario for photometric redshifts, we correctly classify  $\sim 76\%$  of the SNe as type Ia, and improve the scatter in the redshift determination from  $\sigma = 0.3$  to an *a posteriori* value of  $\sigma \sim 0.17$ , thus improving the redshift dispersion by almost a factor of 2. On the other hand, it can clearly be seen that the posterior redshift distribution is heavily biased towards lower  $z$ . This is a consequence of the fact that, the lower the redshift, the more freedom the minimization has in the other parameters. At lower  $z$  the SN template is inherently brighter and can be ‘aged’ and extinguished in order to fit the observed magnitudes, while at higher  $z$  it must be closer to peak and less extinguished.

The most extreme scenario is the absence of any prior on the redshift. This is probably relevant only to the few objects that have no measured host due to its faintness. In this case, we drop to only  $\sim 60\%$  correct classifications, only slightly better than random assignment of SN type. Not surprisingly, parameter space is wide enough to accommodate both types, when no information on the host redshift exists, and the SN light/color curve is so scantily sampled.

We can thus conclude that single epoch photometry in three bands, combined with a reasonably well determined host galaxy redshift, is sufficient to recognize SNe Ia, with only a few false negatives, and high confidence levels.

### 3.1.2. II-P SNe

In order to measure the performance of the SN-ABC in correctly classifying CC-SNe, we repeat the procedure described in §3.1.1, applying the same “pseudo photometric redshifts” to the much smaller sample of five type II-P SNe, presented in Nugent et al. (2006). We

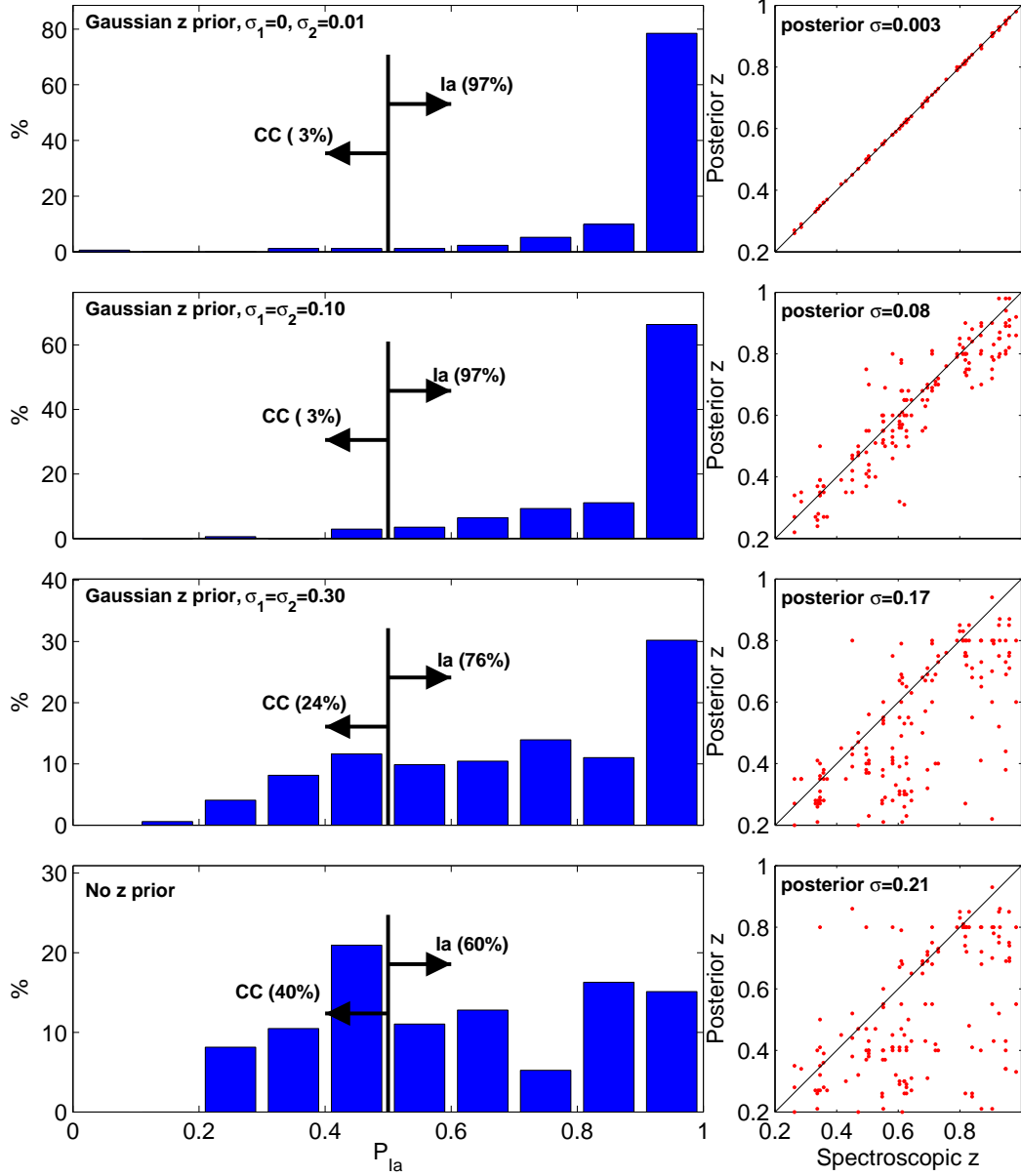


Fig. 1.— Classification of SNe Ia in SNLS. Left, distribution of the type determination parameter  $P_{Ia}$  for different redshift priors. Values of  $P_{Ia}$  higher than 0.5 mean the object is probably a SN Ia, while smaller than 0.5 mean it is a CC-SN. Right, posterior redshifts for the priors on the left. Solid line is  $z_{\text{posterior}} = z_{\text{spec}}$ , for reference. SN-ABC works well assuming good quality photo- $z$  values are available (upper two panels).

extract 25 ‘objects’ with same-day photometry from among three of these SNe, which are at redshifts of 0.13 to 0.21.

As shown in Figure 2, when using the precise spectral redshifts, we achieve a perfect success rate with not a single object misclassified. When using broader, more realistic,  $z$ -pdfs, we reach success rates between 85% ( $\sigma_1 = \sigma_2 = 0.03$ ) and 75% ( $\sigma_1 = \sigma_2 = 0.1$ ). Since the redshifts of these SNe are significantly lower than those of the SNLS Ia sample, we examine cases with comparatively smaller values of  $\sigma_1$  and  $\sigma_2$  that are more reasonable for photometric redshifts in this range.

In all the simulated photo- $z$  schemes we have examined, both for the Ia and CC-SNe, the minimum  $\chi^2$  values are lower than the value that defines the 99% confidence interval on the goodness of fit, which we derive from simulations, as will be described in §4, below. The best fit templates therefore fit the data well in an absolute sense.

While the tests on the SNLS samples, both type Ia and II-P, indicate that our algorithm works well, these results may be misleading since these samples were selected by the SNLS team for their quality, and are not in any sense a complete representation of all the SNe found during the survey. In order to check our method on a complete sample, we apply the SN-ABC to all of the SNe found during the *Hubble Space Telescope* (HST) GOODS campaign.

### 3.2. GOODS

We proceed with a SN sample from the GOODS SN survey. As part of this project, 15 fields of about  $150 \text{ arcmin}^2$  each were observed with the ACS camera on HST every 45 days, over five epochs, in order to search for SNe. We have compiled from Riess et al. (2004a) and Strolger et al. (2004), all available photometry for the 42 SNe found in the GOODS fields. These SNe cover a redshift range of 0.2 to 1.55, with a median of 0.76, which is higher than the SNLS range. The light-curve coverage is more limited than for the SNLS sample, and not all SNe have spectroscopic redshifts or types. However, GOODS is a complete sample, without any subsequent selection. The SNe were classified following a decision scheme presented in Strolger et al. (2004), and the whole sample was divided into three subsets – “gold”, “silver”, and “bronze” – according to the reliability of the type determinations.

As in §3.1, we first reject all the SNe which do not have same day ( $\pm 1$ ) photometry in three bands (in this case F606W, F775W, & F850LP), leaving 28 SNe. After excluding one SN with no redshift information, we extract from the remaining 27 SNe (13 Ia, 14 CC), 41 same-epoch photometry “objects”, of which 23 are of type Ia, and 18 are CC. Among

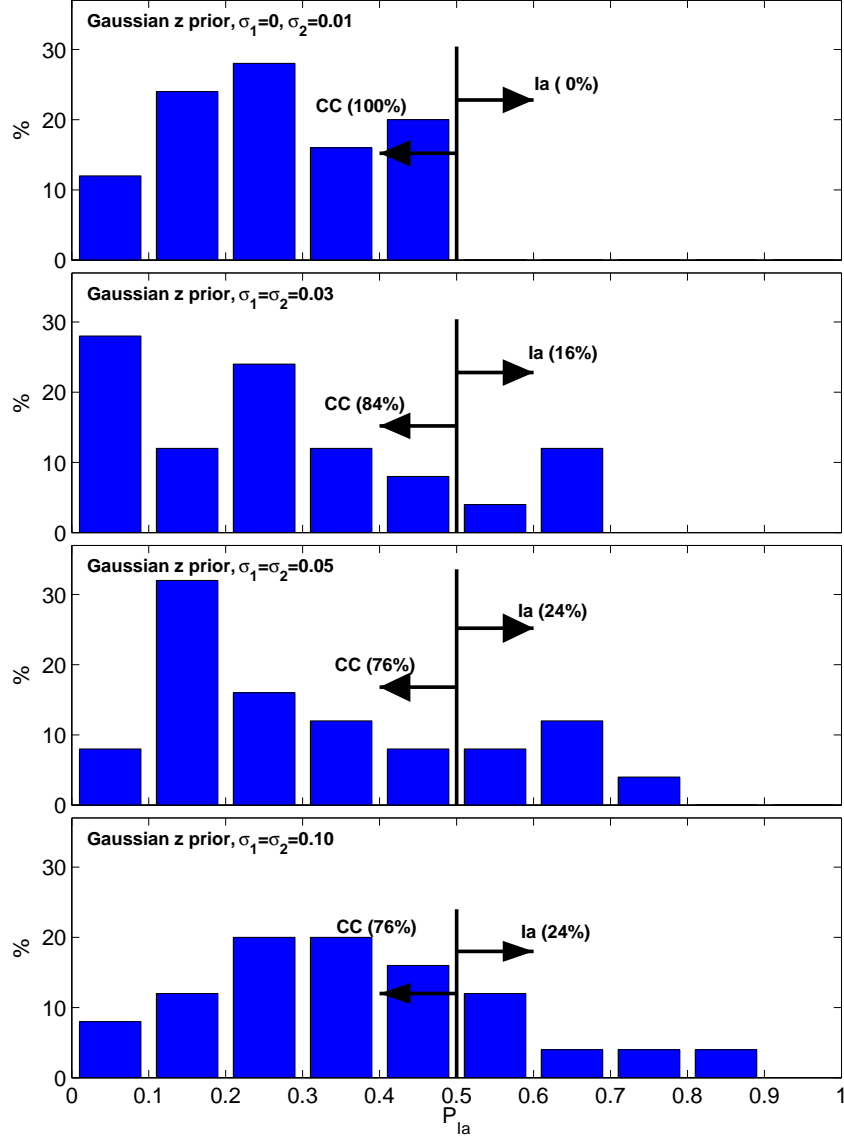


Fig. 2.— Same as Figure 1, for SNLS SNe II-P with four different redshift priors. Values of  $P_{Ia}$  higher than 0.5 mean the object is probably a SN Ia, while smaller than 0.5 mean it is a CC-SN.

these 41 objects, 28 (17 Ia, 11 CC) have spectroscopic redshifts while 13 (6 Ia, 7 CC) have only photometric redshifts. The requirement of same-epoch photometry changes the redshift distribution of the sample, mainly by rejecting the few SNe with  $z > 1$ , and leaves a distribution with a median redshift of  $\sim 0.6$ , ranging from 0.2 to 1, similar to the SNLS Ia sample.

For those SNe with spectroscopic redshifts we create pseudo-photo- $z$ 's, repeating the approach in §3.1, with  $\sigma_1 = \sigma_2 = 0.1$ . When applied to this sample, the SN-ABC correctly classifies 16 of the 17 SNe Ia and 9 of the 11 CC-SNe. The single SN Ia which is misclassified is the last of three observations of SN 2002hr, a SN Ia, about two months past maximum brightness. The previous two epochs of the same SN are well classified. The misclassified CC-SNe are SNe 2002kb and 2003bb. For  $\sigma_1 = 0$ ,  $\sigma_2 = 0.01$ , representing well determined spectral redshifts, the success rates remain unchanged for the CC-SNe, but for the SNe Ia one more object is misclassified, one of the three epochs of SN 2002ga, a bronze SN Ia. Since it is well classified with a broader  $z$ -pdf, its misclassification may be due to an underestimated redshift uncertainty.

For those SNe with photometric redshifts, we assume a Gaussian pdf with  $\sigma_2 = 0.1$ , since we do not have the real  $z$ -pdfs. For this photo- $z$  sample, we recover the same classification as that of the GOODS team for only two of the six SNe Ia and four of the seven CC-SNe. Increasing  $\sigma_2$  to a value of 0.2, to test whether we have underestimated the uncertainty in the redshift, does not improve this result.

It is clear that the SN-ABC functions extremely well on the GOODS SNe with spectroscopic redshifts, mostly in accord with the classification presented in Strolger et al. (2004), while for the SNe with photo- $z$ 's there are severe discrepancies. This illustrates the difficulty to classify SNe without spectroscopy, and it is hard to ascertain which classification scheme is correct for every object. If we consider agreement between the GOODS classification and ours as an indicator of the quality of the classification itself (either the SN-ABC or GOODS), it is clear that our division of the sample according to the existence or non existence of spectral redshift splits the sample into distinct quality classes. This is less true for the GOODS gold/silver/bronze quality flags (though one should note that these divisions are not independent). For example, our classification of the CC-SNe with spectral redshifts, belonging to the bronze sample, is in agreement with the GOODS type for all the objects, while it is in disagreement for one of the four bronze CC-SNe with photo- $z$ . More dramatically, for the silver CC-SNe, neither of the two SNe with photo- $z$  are similarly classified, while four out of the five with spectral redshifts are in agreement. Similar trends are seen with the type-Ia SNe. Since all the SNe Ia in the gold sample have spectral redshifts, this issue has no implications for this particular, higher quality, subset. We note that, by stating that the

subsample with photometric redshifts is of lower quality, we do not imply that the problems arise necessarily from the photometric redshifts themselves, since we do not have the information needed to reveal the source of the discrepancies. The fact that the SN-ABC and GOODS classification for the SNe with spectra are in excellent agreement, shows that our algorithm works well. The fact that there are significant discrepancies when classifying SNe with no spectra indicates that the GOODS classification of at least some of these objects might be erroneous. As in §3.1, there are no objects with minimum  $\chi^2$  values outside the 99% confidence interval.

An advantage of our SN-ABC procedure is that it provides a quantitative indication of the quality of the classification, in the form of the  $P_{Ia}$  value, that can be used for subsequent error estimation. The issues of classification and redshift uncertainties were addressed in Riess et al. (2004a) by deriving separate Hubble diagrams from the gold and silver samples (and ignoring the bronze sample). Dahlen et al. (2004) deal with the uncertainties in the classification only (i.e., ignoring the possible errors in redshift determination), by testing how their results on SN rates change if the entire bronze sample is misclassified. Strolger et al. (2004) used the entire GOODS sample, irrespective of quality, in their derivation of the SN Ia time delay distribution. The latter two treatments do not test for possible biases that arise from errors in classification or redshift determination.

#### 4. Tests on a simulated SN sample

While the GOODS sample is complete, it is quite small and even smaller when restricted to SNe with high confidence classification. This motivates us to explore biases that might arise from our classification algorithm, and the dependence of the success rate on various parameters, by using a large simulated sample of SNe. The simulated sample also permits us to test the performance of the algorithm when the input data are additional CC types, as well as SN “impostors” such as AGNs. For comparison with the results based on the real SN samples, we mimic the observational properties of the GOODS sample with its three HST bandpasses. The results in this section are for this specific configuration. In §4.4 we examine the influence of having more, or less, than three bands on the classification.

We have randomly generated 5,000 SNe of each of the SN types: Ia, Ibc, II-P, and IIn. To each SN we assign a redshift, an epoch, and a host extinction. These characteristics are drawn from a uniform distribution, which facilitates the discovery of possible trends in the reliability of the SN-ABC classification. As in §2.2, we calculate the synthetic magnitudes of the fake SNe using the SEDs from the spectral database of Nugent et al. (2002) for types Ia, Ibc, & II-P SNe. Since the spectra of type IIn SNe in the Nugent et al. (2002) database are

theoretical blackbody SEDs, for this type only we use the templates from Poznanski et al. (2002).

We add intrinsic scatter to every measurement, using the values quoted in §2.2 as standard deviations, with the exception of the color dispersion term for the CC-SNe which we conservatively increase to 0.2, the value used by Sullivan et al. (2006a). We assume the scatter is normally distributed. We have measured the mean photometric errors of the GOODS sample in each band as a function of magnitude, and again assuming the noise is normally distributed, have added it to each object. We further assigned to the SNe a pseudo-photo- $z$  with  $\sigma_1 = \sigma_2 = 0.1$  (see §3.1.1).

#### 4.1. Type Ia SNe

We first investigate the classification success rate as a function of SN age. As can be seen in the top-left panel of Figure 3, the SN-ABC success rate on simulated SN Ia data is very high, greater than 99%, for SNe near maximum, and remaining high,  $\sim 95\%$ , up to about a month past maximum brightness. Most of the SNe in this range are securely classified, with an average  $P_{Ia}$  higher than 0.8. For older SNe, the success rate decreases gradually. This is due to several effects. As shown in Poznanski et al. (2002), SNe Ia at ages of about one to two months have rest-frame UV and blue colors which are similar to those of CC-SNe. These are the colors we observe at high  $z$  in the observer red bands. The older the SN, the fainter it is, and therefore it can be erroneously fitted more easily with younger CC-SN templates, which are intrinsically dimmer.

In the top-right panel of Figure 3 we show the dependence of the success rate on redshift. At low  $z$ , where older SNe Ia can be detected, a redshift uncertainty of 0.1 has a strong influence on the quality of the fit, because of the nonlinear dependence of the luminosity distance on redshift. This means that, by excluding from a sample objects below a certain  $z$ , one can obtain higher classification success rates. The success rate dependence on redshift is further strengthened by the fact that, at higher  $z$ , the SNe are found closer to peak, where they have distinct colors (Gal-Yam et al. 2004). We searched for trends in the success rates of the classification as a function of all the other parameters, such as brightness, color, photometric errors, and extinction, and found no obvious correlation.

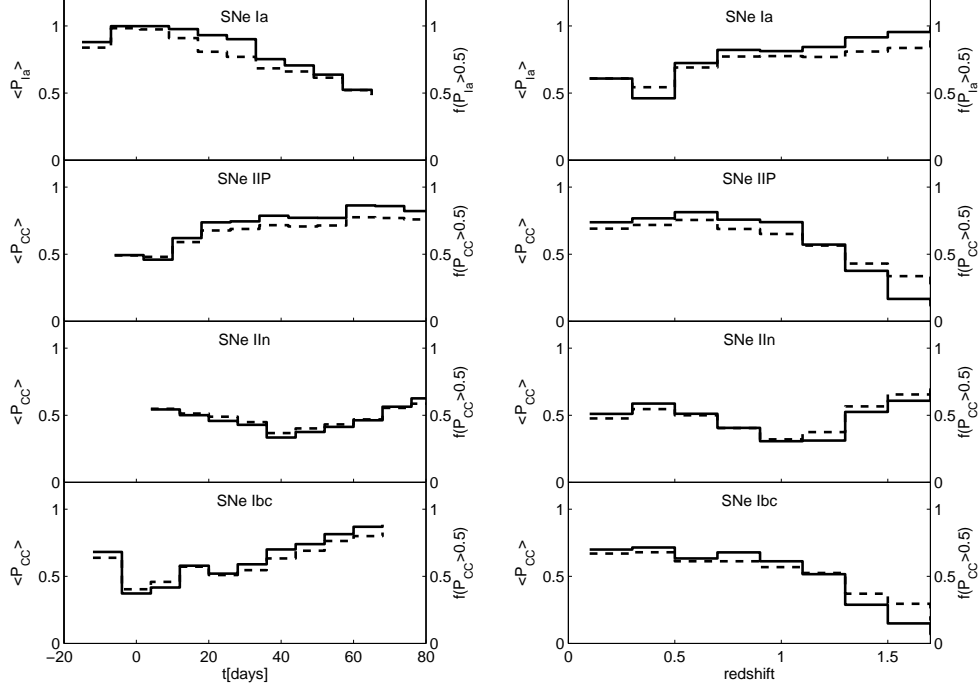


Fig. 3.— Classification results for simulated SNe of types Ia, II-P, Ibc, and IIIn, as marked, observed in three bands. Left: Dashed curves and left axes show the average  $P_{Ia}$  (top panel) or  $P_{CC}$  (bottom three panels) values. Solid curves and right axes show  $f(P_{Ia/CC} > 0.5)$ , the fraction of SNe that are successfully classified (i.e., having  $P_{Ia/CC} > 0.5$ ), as a function of SN age. Note that the two lines are very well correlated, indicating that the SN-ABC output,  $P_{Ia/CC}$ , is a good indicator of the reliability of the classification. Right: Same as left panels, but as a function of redshift.



## 4.2. Core-Collapse SNe

In the six remaining panels of Figure 3, one can see that the picture is more complex within the zoo of CC-SNe. Among type-II-P SNe, 73% are correctly classified, being progressively better classified at later times. This is the complementary image of what we see with type Ia SNe. The colors of young II-P SNe resemble those of Ia SNe about a month past maximum light. For this reason also, type II-P SNe are better classified at low  $z$ .

The SN-ABC fails with type-IIIn SNe, with about half of them being erroneously classified as SNe Ia. This is the result of a degeneracy, in color-magnitude space, between those two types and for which we have no straightforward solution. As already noted in §2.2, we do not use in the SN-ABC a set of type IIIn templates, because their addition, while improving the classification of SNe IIIn as CC-SNe, would considerably hinder SN Ia classification. Type IIIn SNe likely result from the core-collapse of very massive stars (Gal-Yam et al. 2006), the high-mass tail of the initial mass function, and are therefore suppressed in volume limited samples. Cappellaro et al. (1997) measure their fraction to be  $\sim 2 - 5\%$  of the CC population in the local universe. Nonetheless, due to their brightness, in magnitude limited samples their fraction could be as high as  $\sim 15 - 20\%$ . For example, in IAU circulars between January 2005 and September 2006, the Nearby SN factory (Wood-Vasey et al. 2004), and the SDSS II SN survey (Dilday et al. 2005), have together reported  $\sim 11$  type IIIn SNe out of  $\sim 55$  CC-SNe. SNe IIIn appear to be an important contaminant of future SN Ia samples, and may cause difficulties for cosmology oriented studies. This may already have affected some current photometric works, e.g., Barris & Tonry (2006). This contamination might explain their measured SN rates, which seem inconsistent with other published results, as discussed in Neill et al. (2006). The possible contamination of SN-Ia samples by type-IIIn SNe has also been discussed by Germany et al. (2004).

Our algorithm correctly classifies most type Ibc SNe as CC-SNe, but with lower success rates than type II-P SNe, and smaller  $P_{CC}$  values. Considering the fact that we are using II-P templates to recognize Ibc events, this should not be surprising. As with SNe II-P, when SNe Ibc are near peak, their colors are degenerate with those of SNe Ia. The redshift trend of the success rate follows the one we find for type II-P SNe. A caveat is that the templates from which we have simulated the Ibc SNe may not truly represent the high- $z$  population, a possibility that must await future spectroscopy of such events. As was the case for SNe Ia, we find no trends in the SN-ABC results as a function of all the other simulated parameters, such as magnitudes in the different bands, photometric errors, and extinction.

Finally, we have calculated for each of the simulated SNe the  $\chi^2$  value for the best fitting SN template. The  $\chi^2$  distribution for each of the SN types can be seen in Figure 4. The distribution is similar to the expected  $\chi^2$  probability density function with one degree

of freedom. Had our model been linear, and its parameters non-degenerate, we would have expected to have zero degrees of freedom, since we fit three parameters (redshift, age, and extinction) to three data points per object (the magnitudes in three bands). Fortunately, our model is non-linear, and has some degeneracies between the parameters, so that useful information can be extracted as we have shown. From the distribution of  $\chi^2$  values in the simulations, we can derive the 99% confidence interval, which can be used to reject objects which are poorly fit by all of our models. Such objects could be peculiar types of SNe or SN impostors (e.g., AGNs, the major contaminant in SN surveys) with significantly different colors. In SNLS and GOODS, all the SNe we examined had  $\chi^2$  smaller than the 99% confidence limit of the simulated dataset, meaning there were no true SNe that were misclassified as peculiar/impostor SNe. In our application of SN-ABC to a real “spectroscopically blind” SN survey, we can use the  $\chi^2$  criterion to assess the contamination by peculiar events and by AGNs. We test this on simulated AGNs in the following section.

### 4.3. AGN Rejection

Using the same approach used to simulate a SN sample, we have generated 400 mock AGNs using as a template the composite AGN spectrum from Vanden Berk et al. (2001), and a redshift dependent luminosity function from Boyle et al. (2000). We have extrapolated the function to low luminosities based on the evidence presented in Wolf et al. (2003). We expect, at least in some cases, the photometric redshift to fail due to the contribution of the AGN to the colors of the host galaxy. As an approximation of this effect, we generate for each AGN a random host galaxy drawn from a Schechter distribution (Schechter 1976). If the AGN luminosity is smaller than the galaxy’s, we assume the photo- $z$  works well, and otherwise we generate a completely random photo- $z$ . Among the AGNs, 265 are first classified as CC-SNe according to their  $P_{Ia}$  values, and the remaining 135 as SNe Ia. After applying a  $\chi^2$  cut, at the 95% confidence limit, 189 of the CC impostors are rejected, but only eight of the Ia impostors. There is no significant difference between the samples with ‘good’ and ‘bad’ photometric redshifts, so our approximation for the redshift determination is inconsequential.

Thus, we can reject more than half of the AGNs we simulate. The remaining objects contaminate in about equal fractions the Ia and CC-SN samples. Note that in any search that includes more than two epochs, most of these AGNs will be rejected due to their non-SN-like variability, and survey-specific simulations can be carried out to test for the existence of residual contamination.

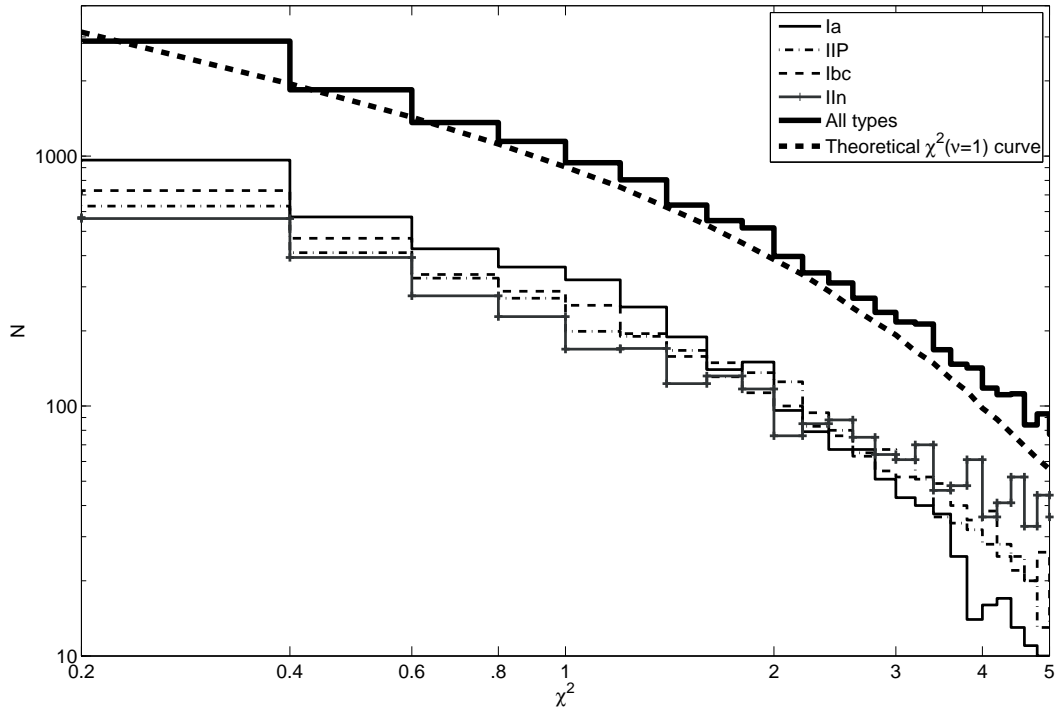


Fig. 4.—  $\chi^2$  distributions for the sample of simulated SNe, by type and for all types combined, compared to the expected distribution with one degree of freedom.

#### 4.4. Number of Photometric Bands

We have studied the performance of the SN-ABC in classifying SNe with single-epoch photometry in three bands. we now examine the improvement, or degradation, of the classification success rate for surveys using more or fewer bands.

We begin with the addition of observations in a fourth, bluer, band, specifically the HST F475W filter. We repeat the simulations presented in the previous sections, though with fewer SNe (500 of each type), due to computational limitations. Comparing the results shown in Figure 5 to those obtained with three bands in Figure 3, one can see that although there is some improvement, it is not striking. The overall success rate for SNe Ia improves from 82% to 88%, but at a young age remains similar, at 95%. This improvement is mainly for older SNe, at low redshift. As can be seen in the six bottom panels of Figure 5, for the CC-SNe of the different subtypes, the improvement in these cases is even less significant, and is null for type-IIIn SNe.

In order to test whether this improvement remains marginal for real data, we used the SNLS sample which has  $g$  band observations for some of the SNe. We repeated the process described in §3.1.1, with the fourth band added, and  $\sigma_1 = \sigma_2 = 0.1$ . In this case 99% of the Ia SNe are correctly classified (only one misclassified), with 74% having  $P_{Ia} > 0.9$ . While this is better than with three bands, it is not a dramatic improvement. For  $\sigma_1 = \sigma_2 = 0.3$ , the correctly classified fraction of SNe Ia rises from 76% with three bands to 84% with four. The SNe II-P are only marginally better classified, but the sample with observations in four bands consists of only eight such objects. We thus conclude that for classification purposes, when the photometric redshifts are reasonably good, observations in a fourth band may be an inefficient use of telescope time.

Next, we examine the success rate of the SN-ABC when using observations only in two bands. Since the best bands for high- $z$  SN observations are the reddest, we discard the bluest band, and remain with F775W and F850LP. As expected, with two bands the results, shown in Figure 6, are degraded. Nonetheless, in some regions of parameter space, the success rate of the SN-ABC is non-negligible. SNe Ia show the same change as when dropping from four bands to three. The success rates drop especially at low redshift and for old ages. The overall success rate for SNe Ia is reduced to 70%. On the other hand, surprisingly, the success rate for II-P and Ibc SNe is actually higher with two bands than with three. This could be understood in the following way. As described in §2.2, our model for the absolute magnitude of CC-SNe includes a much greater dispersion than that of SNe Ia, in order to account for their intrinsic diversity. This entails that CC-SNe can populate wider volumes of color-magnitude space, so that when observational constraints are weak (with one or two bands observed) summing the likelihood over all parameter space makes the evidence  $E_{CC}$

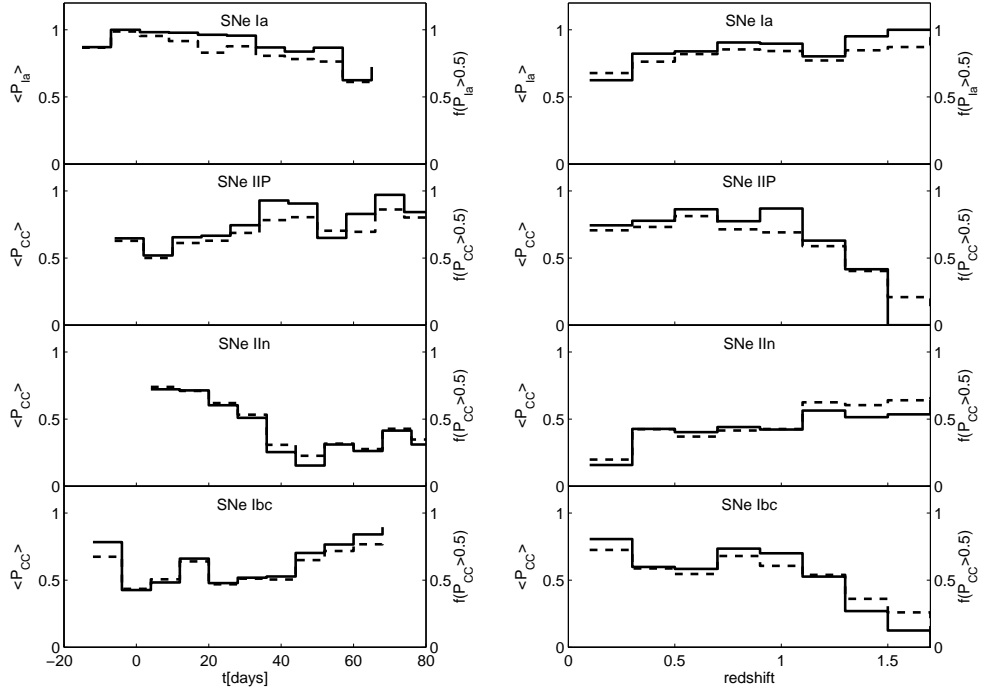


Fig. 5.— Same as Figure 3, for simulated SNe observed in four bands.

greater on average than  $E_{Ia}$ , and thus increases  $P_{CC}$  for all objects, regardless of their real type. As a consequence SN Ia classification is hindered, while CC-SNe are apparently better classified. We tested this explanation by reducing artificially the dispersion of CC-SNe in our model. As a consequence, SN Ia classification improved dramatically, regardless of the number of observed bands, while CC-SN classification success was accordingly reduced, being worst with the least number of bands.

Even with only one observed band (the reddest, F850LP), as can be seen in Figure 7, the SN-ABC manages to classify successfully some SNe, e.g. 75-85% of the SNe with redshifts  $z > 0.7$ , excluding SNe IIn. This is mainly due to the fact that, at least in our models, SNe Ia are significantly brighter than CC-SNe, which is enough to differentiate (probabilistically) between Ia and CC-SNe when the redshift is constrained.

Finally, AGN rejection, while improving only marginally when adding a fourth band, is weakened considerably when discarding information in one or two bands. This comes from the longer tail of high values that the  $\chi^2$  distributions have in these cases. Such a tail increases the 95% confidence limit by a factor of ten, when compared to the scenarios with three or four bands, and does not allow the rejection of any AGNs.

Thus, while some classification can be done with one or two photometric bands, the biases in the resulting samples are stronger and the success rates are rather low. On the other hand, four bands seem not to be worth the extra observing time, over observations in three bands, if the sole purpose is to classify the SNe based on single-epoch data. This also suggests that, with better sampled light curves, the added value of a blue fourth band is small.

## 5. Conclusions

Using the SN-ABC, a Bayesian algorithm, we have demonstrated the feasibility of automatic classification of SNe, based solely on single-epoch multiband photometry and prior redshift information. We have tested our technique on samples of SNe from the SNLS and GOODS projects that have spectroscopic classification, and on artificial datasets. For most samples and settings our method functions very well, with high success rates. When assuming reasonably-well-established photometric redshifts, the SN-ABC correctly classifies 97% of the type-Ia SNe from SNLS, and 85% of the type II-P SNe. Similar numbers are achieved for a subset of the GOODS SNe for which there are spectroscopic redshifts. Using tests on artificial samples we have shown that SNe Ia are best recognized at  $z \gtrsim 0.6$ , or when near maximum, with success rates of the order of 95%. Core-collapse SNe are best classified

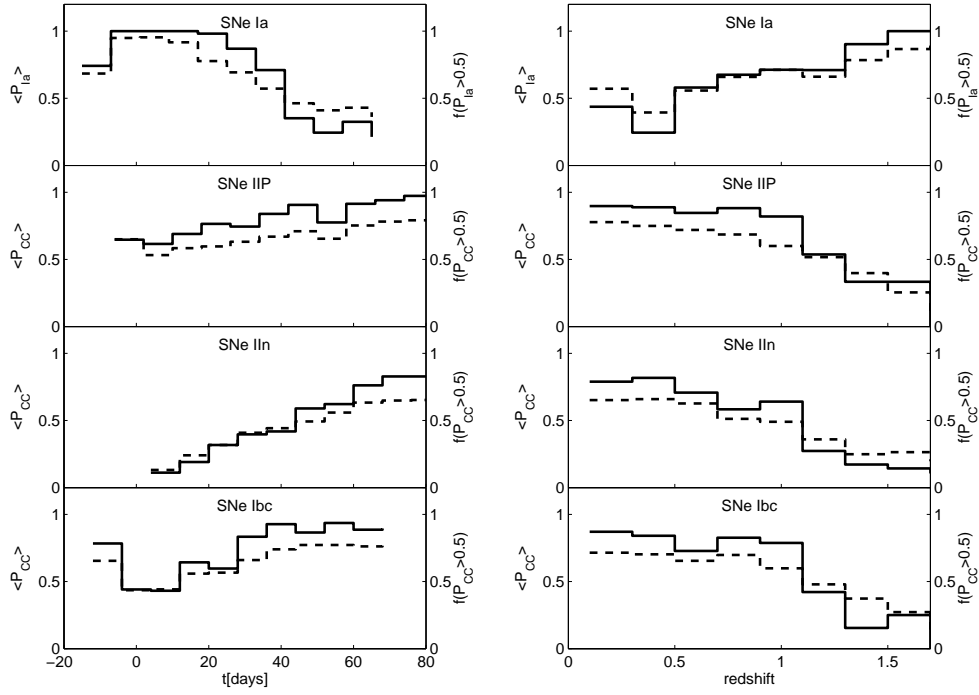


Fig. 6.— Same as Figure 3, for simulated SNe observed in two bands (F775W and F850LP).

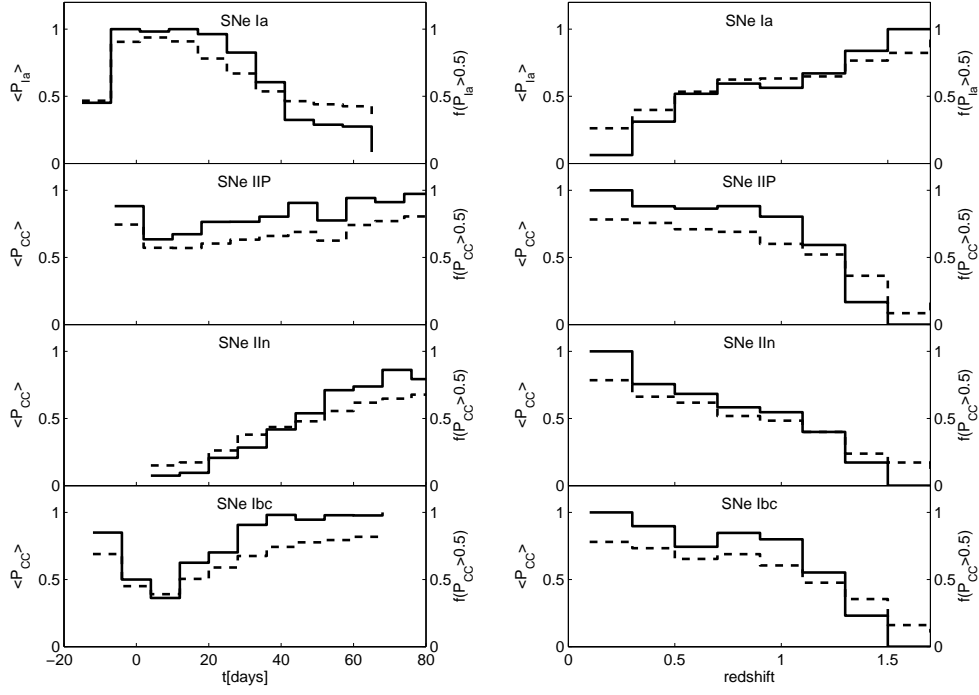


Fig. 7.— Same as Figure 3, for simulated SNe observed in one band (F850LP).



several weeks after maximum, or at  $z \lesssim 0.6$ . An additional feature of the SN-ABC is the ability to reject SN “impostors”, mainly AGNs, using  $\chi^2$  statistics. In our simulations half of the AGNs we simulated were rejected when using a  $\chi^2$  confidence limit of 95%.

While we have focused on SNe observed in three bands, we have found that a fourth band may be of little influence for the purpose of classification, while with fewer bands some objects may still be classified, even when observed in a single band. AGN rejection, though, fails with less than three bands. In all the cases studied, the output values, which we use to classify the SNe,  $P_{CC}$  and  $P_{Ia}$ , are also indicative of the quality of the fit, and the reliability of the result. As can be seen in Figures 3 and 5-7, the mean values of  $P_{CC}$  and  $P_{Ia}$  follow the success rate of the SN-ABC, indicating that indeed these are good quality indicators, and could be used both to define subsamples with lower uncertainties, and to estimate confidence intervals. Since the SN-ABC classification success is dependent on the specific observational setup and on the SN sample characteristics, any statistical use of its output requires a careful investigation of possible biases in the relevant scenario. Such methods are prerequisite for pushing the exploration of the SN population to fainter magnitudes and higher redshifts.

We thank the SNLS team, specifically R. Pain and P. Nugent, for access to SNLS data, and S. Leach, E. O. Ofek, and K. Sharon, for useful discussions. A.G. acknowledges support by NASA through Hubble Fellowship grant #HST-HF-01158.01-A awarded by STScI, which is operated by AURA, Inc., for NASA, under contract NAS 5-26555.

## REFERENCES

- Aldering, G. 2005, *New Astronomy Review*, 49, 346
- Astier, P. et al. 2006, *A&A*, 447, 31
- Barris, B. J., & Tonry, J. L. 2004, *ApJ*, 613, L21
- . 2006, *ApJ*, 637, 427
- Benítez, N. 2000, *ApJ*, 536, 571
- Boyle, B. J., Shanks, T., Croom, S. M., Smith, R. J., Miller, L., Loaring, N., & Heymans, C. 2000, *MNRAS*, 317, 1014
- Cappellaro, E. et al. 2005, *A&A*, 430, 83
- Cappellaro, E., Turatto, M., Tsvetkov, D. Y., Bartunov, O. S., Pollas, C., Evans, R., & Hamuy, M. 1997, *A&A*, 322, 431
- Cardelli, J. A., Clayton, G. C., & Mathis, J. S. 1989, *ApJ*, 345, 245
- Coe, D., Benítez, N., Sánchez, S. F., Jee, M., Bouwens, R., & Ford, H. 2006, *AJ*, 132, 926
- Dahlén, T., & Fransson, C. 1999, *A&A*, 350, 349
- Dahlen, T. et al. 2004, *ApJ*, 613, 189
- Dilday, B. et al. 2005, *BAAS*, 37, 1459
- Elmhamdi, A., Chugai, N. N., & Danziger, I. J. 2003, *A&A*, 404, 1077
- Filippenko, A. V. 1997, *ARA&A*, 35, 309
- Filippenko, A. V., Li, W. D., Treffers, R. R., & Modjaz, M. 2001, in *ASP Conf. Ser. 246: IAU Colloq. 183: Small Telescope Astronomy on Global Scales*, ed. B. Paczynski, W.-P. Chen, & C. Lemme, 121
- Förster, F., Wolf, C., Podsiadlowski, P., & Han, Z. 2006, *MNRAS*, 368, 1893
- Fukugita, M., Ichikawa, T., Gunn, J. E., Doi, M., Shimasaku, K., & Schneider, D. P. 1996, *AJ*, 111, 1748
- Gal-Yam, A., Cenko, S. B., Fox, D. W., Leonard, D. C., Moon, D.-S., Sand, D. J., & Soderberg, A. M. 2005, in *ASP Conf. Ser. 342: 1604-2004: Supernovae as Cosmological Lighthouses*, ed. M. Turatto, S. Benetti, L. Zampieri, & W. Shea, 305

- Gal-Yam, A. et al. 2006, *apJ*, submitted, astro-ph/0608029
- Gal-Yam, A., & Maoz, D. 2004, *MNRAS*, 347, 942
- Gal-Yam, A., Poznanski, D., Maoz, D., Filippenko, A. V., & Foley, R. J. 2004, *PASP*, 116, 597
- Gelman, A., Carlin, J., Stern, H., & Rubin, D. 1995, *Bayesian Data Analysis* (Chapman & Hall)
- Germany, L. M., Reiss, D. J., Schmidt, B. P., Stubbs, C. W., & Suntzeff, N. B. 2004, *A&A*, 415, 863
- Grazian, A. et al. 2006, *A&A*, 449, 951
- Hillebrandt, W., & Niemeyer, J. C. 2000, *ARA&A*, 38, 191
- Jha, S. et al. 2006, *AJ*, 131, 527
- Johnson, B. D., & Crotts, A. P. S. 2006, *AJ*, 132, 756
- Kaiser et al. 2005, *BAAS*, 37, 1409
- Kashikawa, N. et al. 2004, *PASJ*, 56, 1011
- Kuznetsova, N. V., & Connolly, B. M. 2006, *phy Rev D*, submitted, astro-ph/0609637
- Li, W., Filippenko, A. V., Treffers, R. R., Riess, A. G., Hu, J., & Qiu, Y. 2001, *ApJ*, 546, 734
- Mannucci, F., Della Valle, M., & Panagia, N. 2006, *MNRAS*, 370, 773
- Mannucci, F., Della Valle, M., Panagia, N., Cappellaro, E., Cresci, G., Maiolino, R., Petrosian, A., & Turatto, M. 2005, *A&A*, 433, 807
- Maoz, D., & Gal-Yam, A. 2004, *MNRAS*, 347, 951
- Neill, J. D. et al. 2006, *AJ*, 132, 1126
- Nobili, S., Goobar, A., Knop, R., & Nugent, P. 2003, *A&A*, 404, 901
- Nugent, P., Kim, A., & Perlmutter, S. 2002, *PASP*, 114, 803
- Nugent, P. et al. 2006, *ApJ*, 645, 841

- Poznanski, D., Gal-Yam, A., Maoz, D., Filippenko, A. V., Leonard, D. C., & Matheson, T. 2002, *PASP*, 114, 833
- Rajala, A. M. et al. 2005, *PASP*, 117, 132
- Richardson, D., Branch, D., Casebeer, D., Millard, J., Thomas, R. C., & Baron, E. 2002, *AJ*, 123, 745
- Riess, A. G. et al. 2004a, *ApJ*, 607, 665
- . 2004b, *ApJ*, 600, L163
- Scannapieco, E., & Bildsten, L. 2005, *ApJ*, 629, L85
- Schechter, P. 1976, *ApJ*, 203, 297
- Schlegel, D. J., Finkbeiner, D. P., & Davis, M. 1998, *ApJ*, 500, 525
- Sollerman, J. et al. 2005, *astro-ph/0510026*
- Strolger, L.-G. et al. 2004, *ApJ*, 613, 200
- Stubbs, C. W., Sweeney, D., & Tyson, J. A. 2004, *BAAS*, 36, 1527
- Sullivan, M. et al. 2006a, *AJ*, 131, 960
- . 2006b, *ApJ*, 648, 868
- Tonry, J. L. et al. 2003, *ApJ*, 594, 1
- Vanden Berk, D. E. et al. 2001, *AJ*, 122, 549
- Wolf, C., Wisotzki, L., Borch, A., Dye, S., Kleinheinrich, M., & Meisenheimer, K. 2003, *A&A*, 408, 499
- Wood-Vasey, W. M. et al. 2004, *New Astronomy Review*, 48, 637
- Woosley, S., & Janka, T. 2005, *Nature Physics*, 1, 147